Supporting Information For

# Vanadium Oxide Integrated on Hierarchically Nanoporous Copper for Efficient Electroreduction of $CO_2$ to Ethanol

*Qingcheng Yang,[a] Xunlin Liu,[a] Wei Peng,[a] Yang Zhao,[a] Zhixiao Liu,[a]* Ming Peng,[a] Ying-Rui Lu,[b] Ting-Shan Chan,[b] Xiandong Xu,[a] Yongwen Tan[a]**

[a]College of Materials Science and Engineering, Hunan University, Changsha, Hunan 410082, China.

[b]National Synchrotron Radiation Research Center, Hsinchu 300, Taiwan

**Corresponding Author**

*E-mail: zxliu@hnu.edu.cn; tanyw@hnu.edu.cn

**Supplementary Figures**

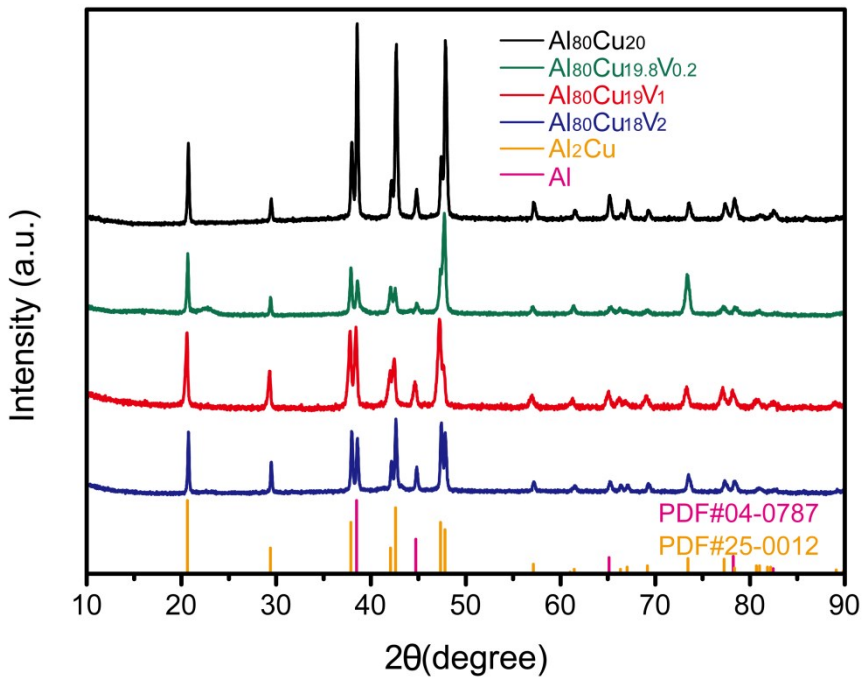


**Figure S1.** The XRD patterns of the precursor $Al_{80}Cu_{20}$, $Al_{80}Cu_{19.8}V_{0.2}$, $Al_{80}Cu_{19}V_1$, and $Al_{80}Cu_{18}V_2$.

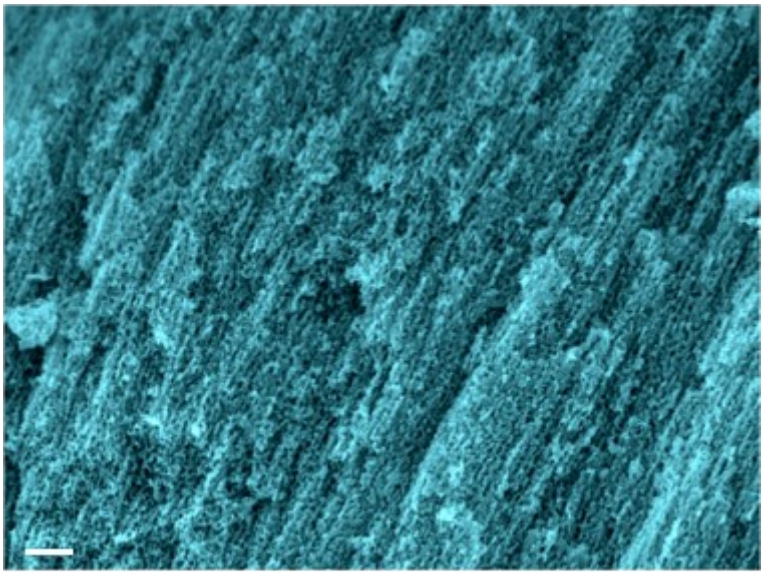

**Figure S2.** High magnification cross-section SEM images of np-Cu@$VO_2$-5%. Scale bar: 1 um.

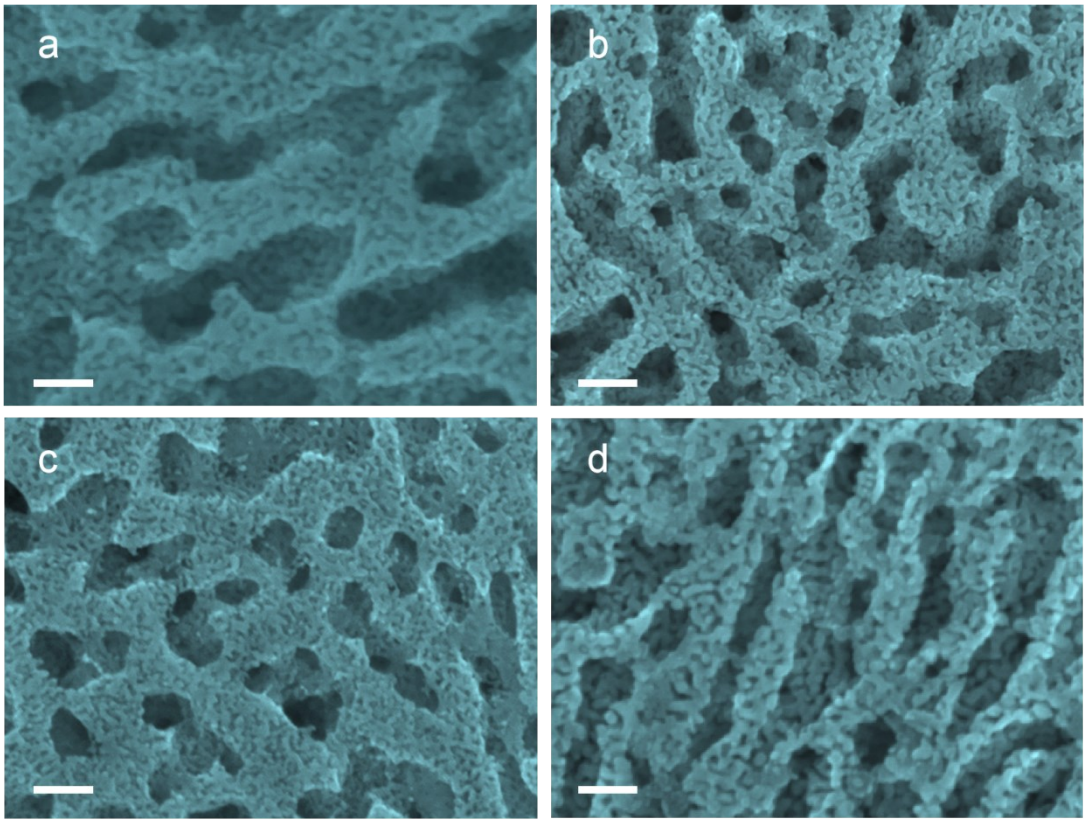


**Figure S3.** The SEM images of (a) np-Cu (b) np-Cu@$VO_2$-1% (c) np-Cu@$VO_2$-10%. (d) np-Cu@$VO_2$-5% after 12h $CO_2$RR testing. Scale bars: (a-c) 100 nm.

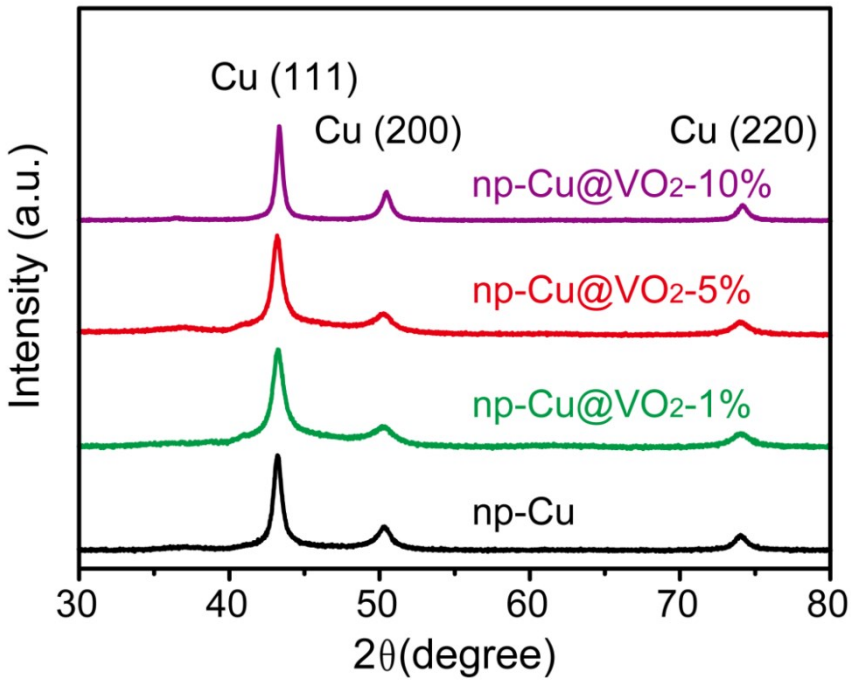


**Figure S4.** The XRD patterns for np-Cu and np-Cu@$VO_2$-M% (M=1, 5, 10).

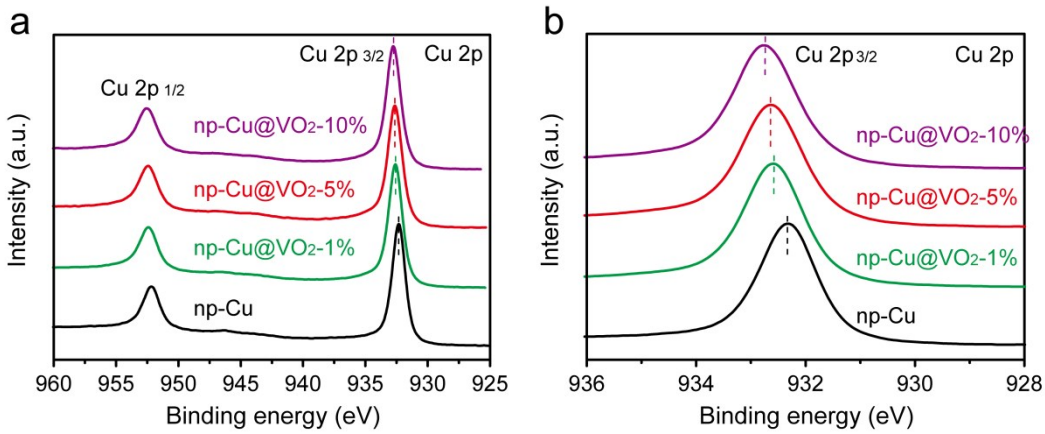


**Figure S5.** (a) Cu 2p and (b) Cu 2p-amplification offset XPS spectra of np-Cu and np-Cu@$VO_2$-M% (M=1, 5, 10).

The Cu 2p track spectrum of np-Cu@$VO_2$-M% (M=1, 5, 10) has two peaks with the nearby binding energies of 932.3 and 952.4 eV, corresponding to $Cu^0$ $2p_{3/2}$ and $Cu^0$ $2p_{1/2}$ respectively. This is coincided with the XRD results that oxides-phase of

copper did not exist. After enlarging the Cu 2p spectrogram, it can be clearly seen that the Cu 2p has a positive shift of 0.3 eV in the np-Cu@$VO_2$-1% samples compared to np-Cu, indicating the existence of electronic interaction between copper skeleton and vanadium atom. For np-Cu@$VO_2$-5%, there are two peaks located at 932.7 eV and 952.8 eV, corresponding to Cu $2p_{3/2}$ and Cu $2p_{1/2}$ of $Cu^0$. Compared with np-Cu@$VO_2$-1%, only a slight positive shift for Cu $2p_{3/2}$ and Cu $2p_{1/2}$ of np-Cu@$VO_2$-5% can be found. It is clear that the Cu 2p XPS peaks spectra shifts to high energy with the increase of vanadium content.

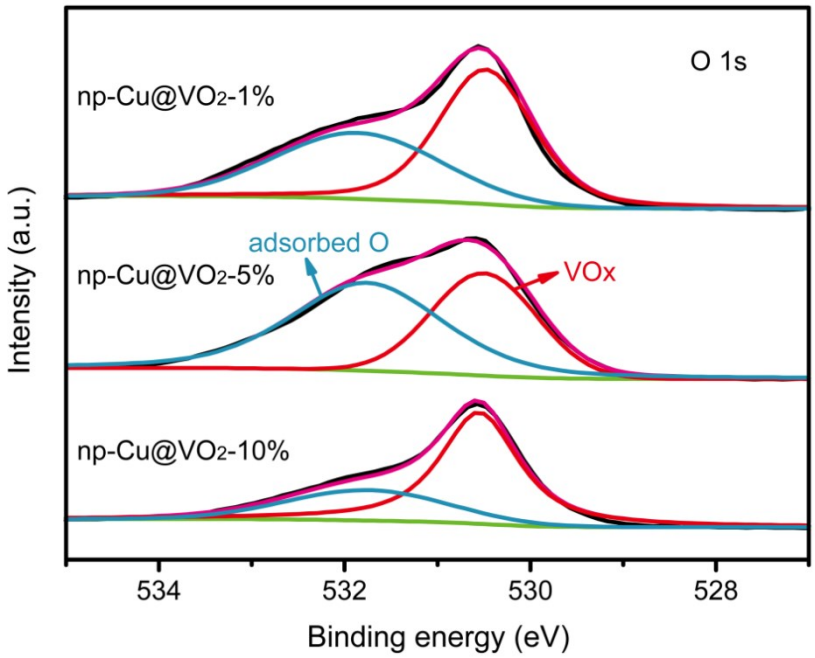


**Figure S6.** O 1s XPS spectra of np-Cu@$VO_2$-1%, np-Cu@$VO_2$-5% and np-Cu@$VO_2$-10%.

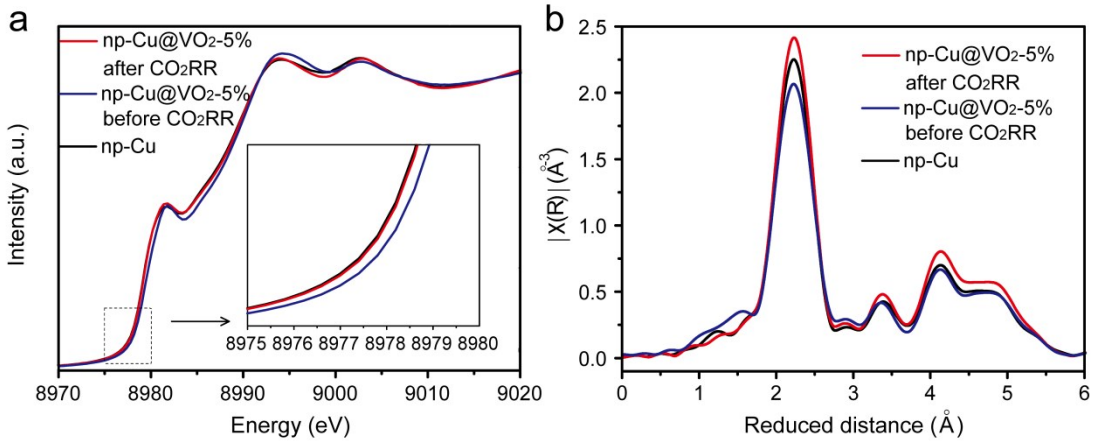


**Figure S7.** (a) Cu K-edge XANES spectra and (b) FT of the EXAFS spectra for np-Cu and np-Cu@$VO_2$-5% before and after $CO_2$RR reaction.

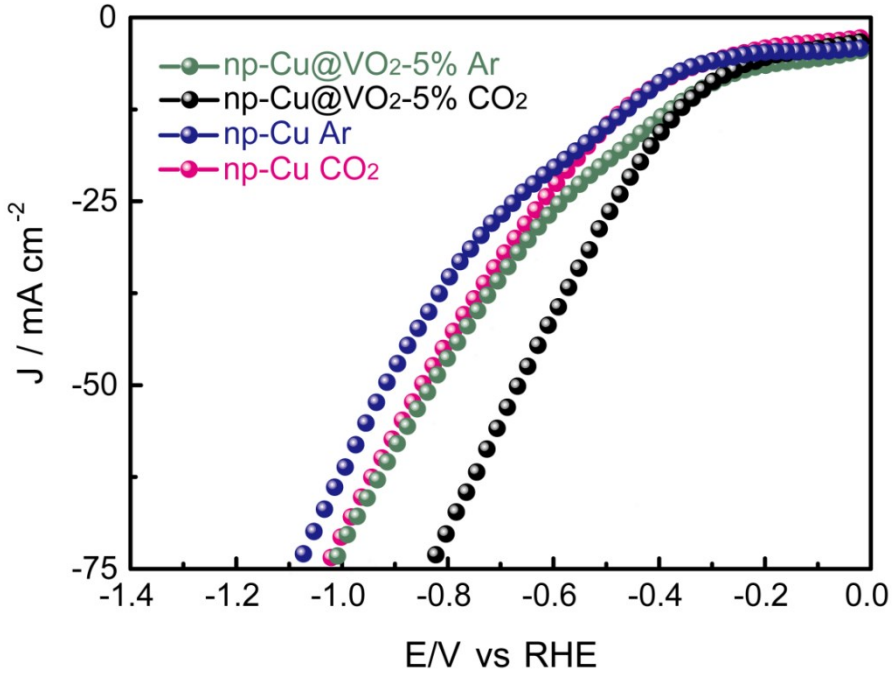


**Figure S8.** Polarization curves of np-Cu and np-Cu@$VO_2$-5% in H-type cell under Ar and $CO_2$-saturated solution (Scan rate: 50 mV/s).

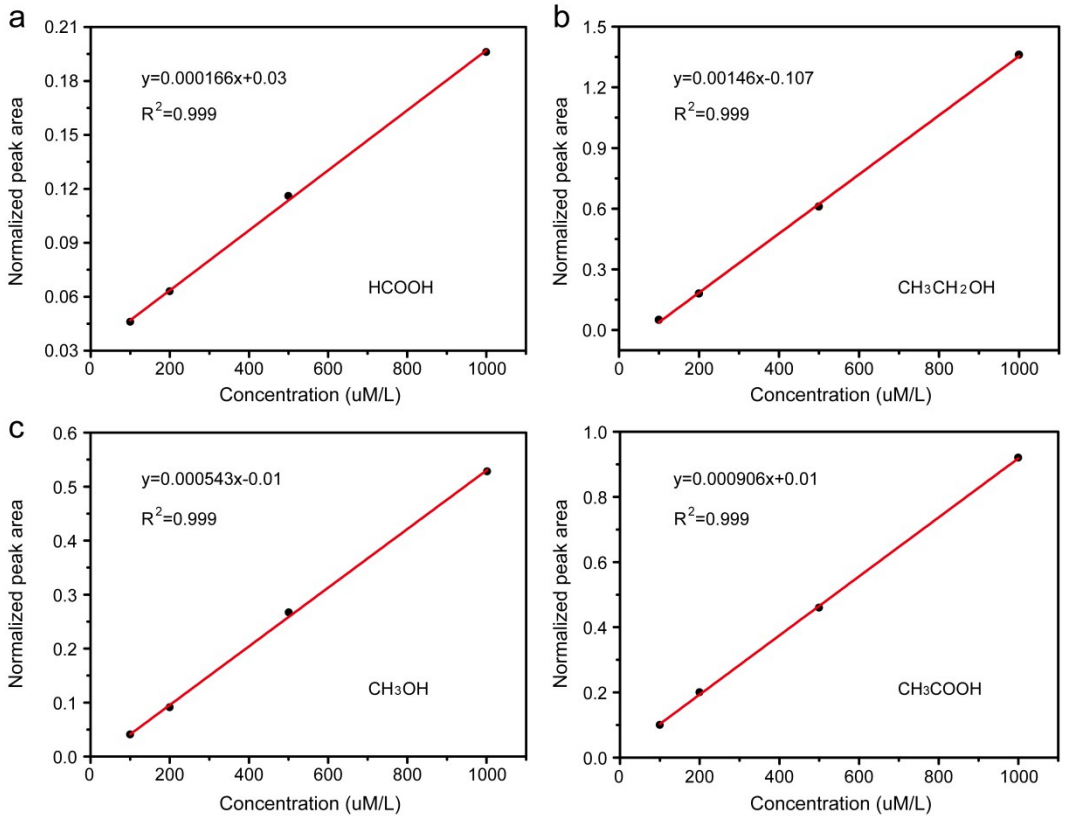


**Figure S9.** External standard calibration curve used for quantification of $CO_2$ reduction products. DMSO (dimethyl sulfoxide) is used as an internal standard for accurate quantitative liquid products. Normalize peak area was the ratio of product peak area to internal standard DMSO area. (a) HCOOH. (b) $CH_3CH_2OH$. (c) $CH_3OH$. (d) $CH_3COOH$.

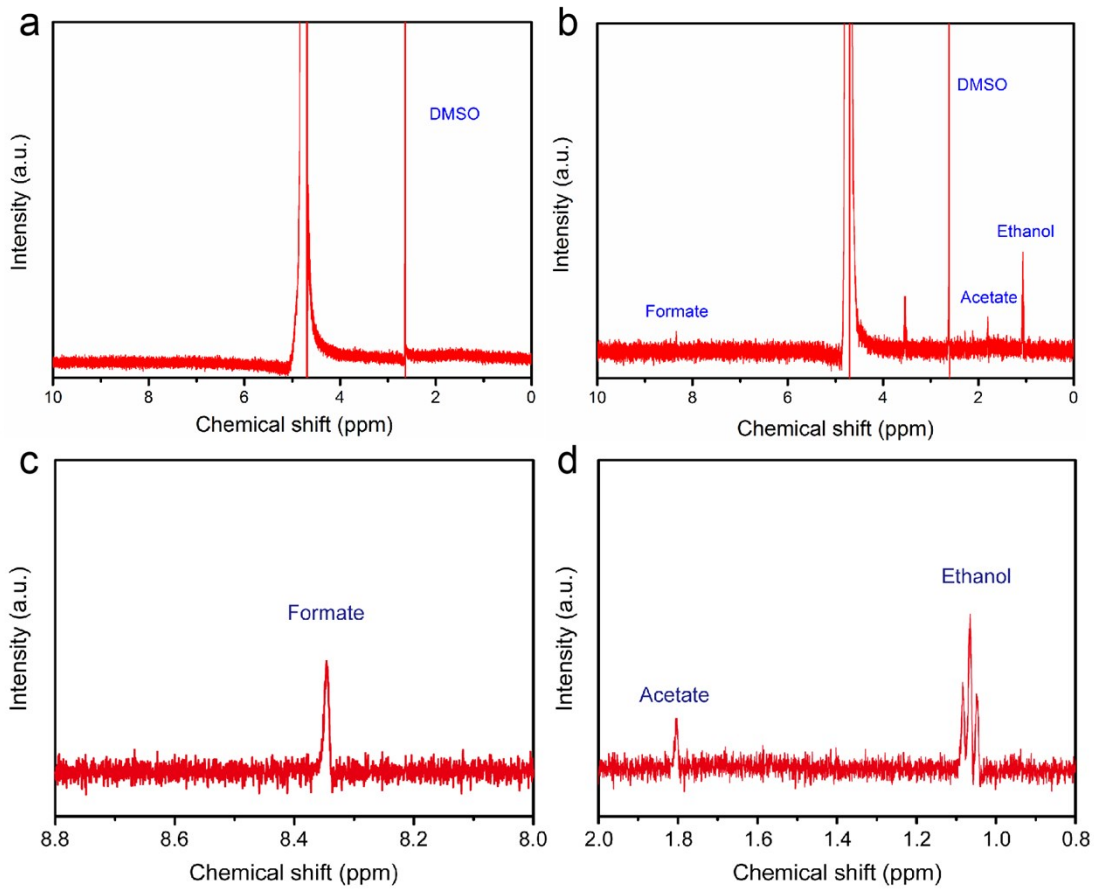


**Figure S10.** $^{1}H$ nuclear magnetic resonance spectra. (a) and (b) Representative $^{1}H$ NMR spectrum obtained from the 1.0 M KOH electrolyte of $CO_2$ reduction on np-Cu@$VO_2$-5% catalyst at open circuit voltage and -0.82 V *vs* RHE in flow cell. DMSO (dimethyl sulfoxide) is used as an internal standard for accurate quantitative liquid products. (c) Local amplification of product formic acid chemical shift. (d) Local amplification of product ethanol and acetate chemical shift.

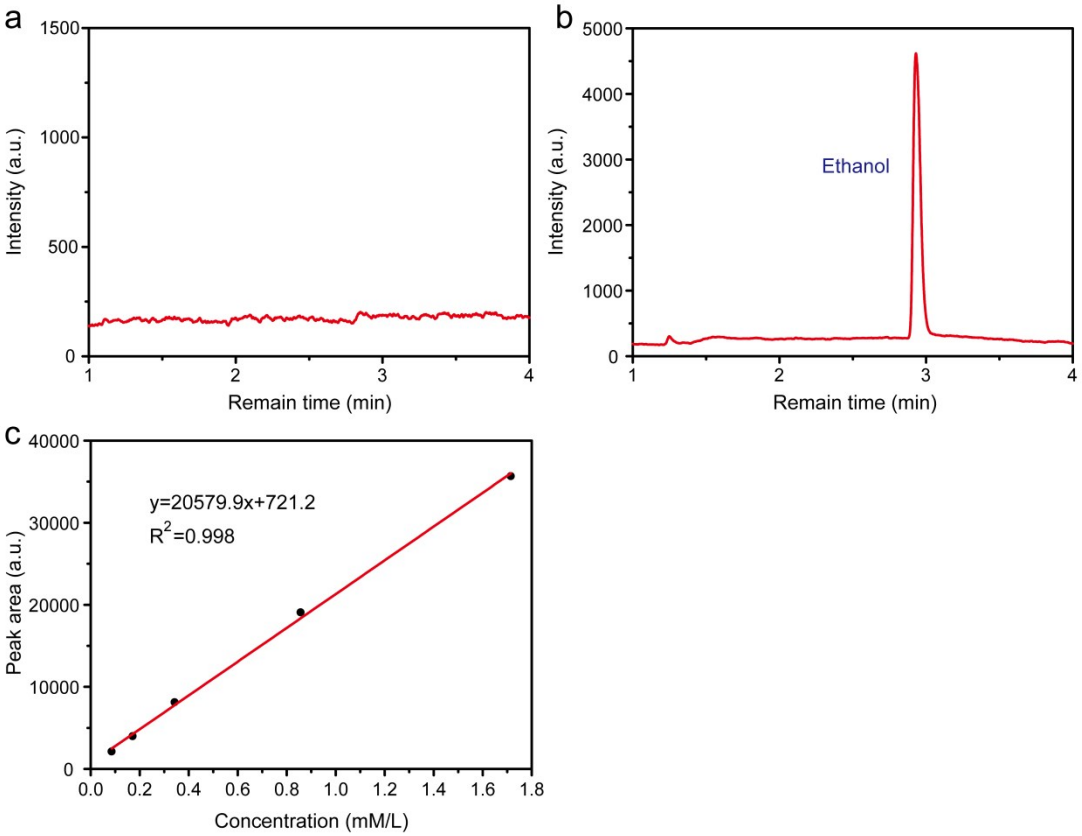


**Figure S11.** (a) and (b) Representative chromatogram obtained from the 1.0 M KOH catholyte after $CO_2$ reduction on np-Cu@$VO_2$-5% catalyst at open circuit voltage and -0.82 V *vs*. RHE in flow cell, respectively. The detection temperature of chromatographic column is 150 ℃. (c) External standard calibration curve used for quantification of $CO_2$RR product $C_2H_5OH$ detected by GC.

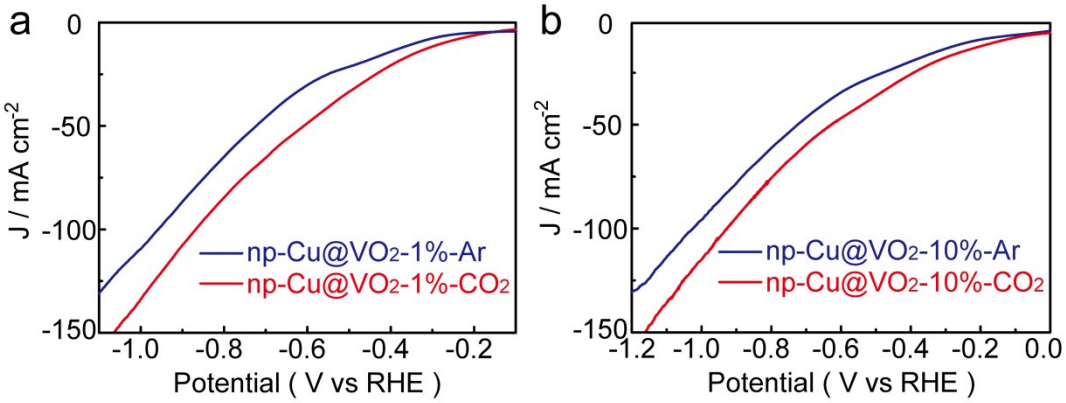


**Figure S12.** Comparison of polarization curves of (a) np-Cu@$VO_2$-1% and (b) np-

Cu@$VO_2$-10% under Ar and $CO_2$-saturated solution.

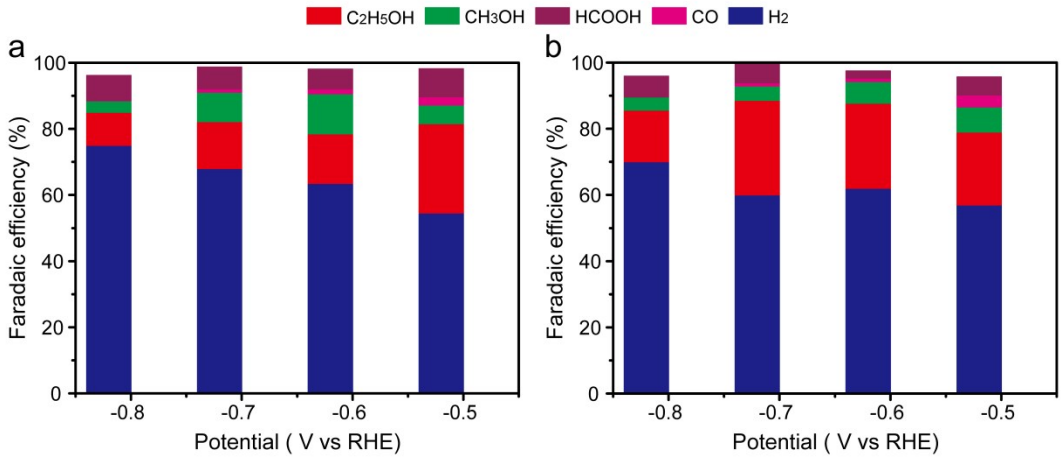


**Figure S13.** The faraday efficiency of main products for (**a**) np-Cu@$VO_2$-1% and (**b**) np-Cu@$VO_2$-10% at different specific potential in H-type cell.

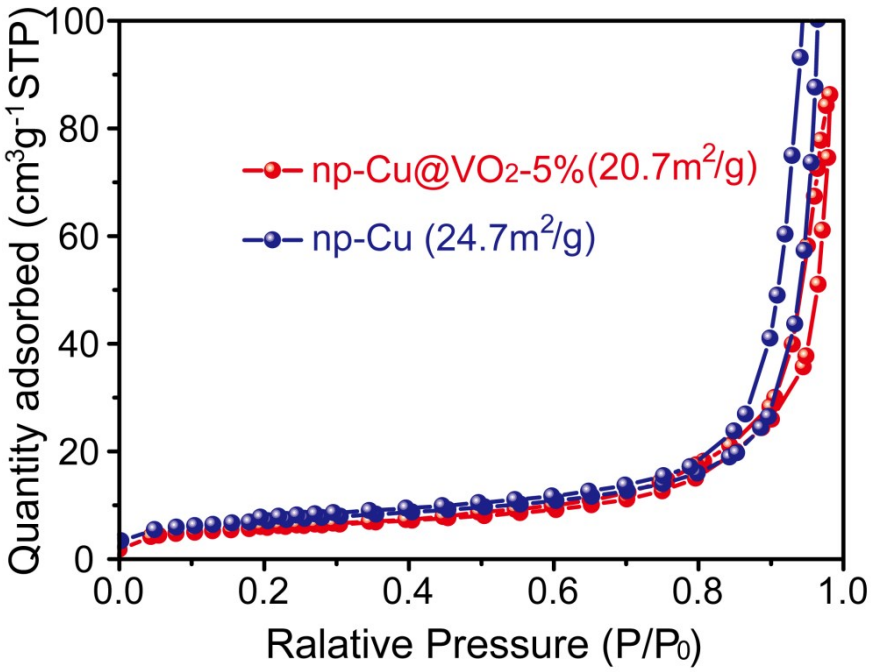


**Figure S14.** $N_2$ adsorption-desorption isotherms at 77 K of np-Cu@$VO_2$-5% and np-Cu.

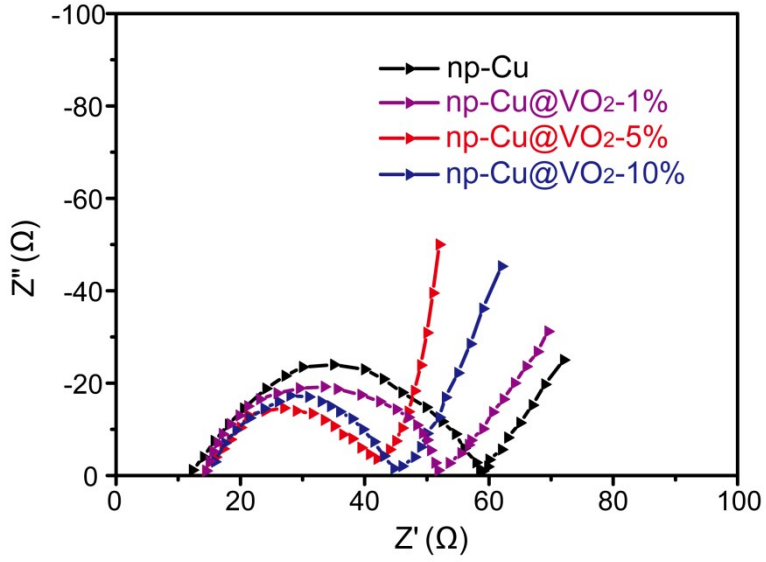


**Figure S15.** Nyquist plots of np-Cu and np-Cu@$VO_2$ electrodes

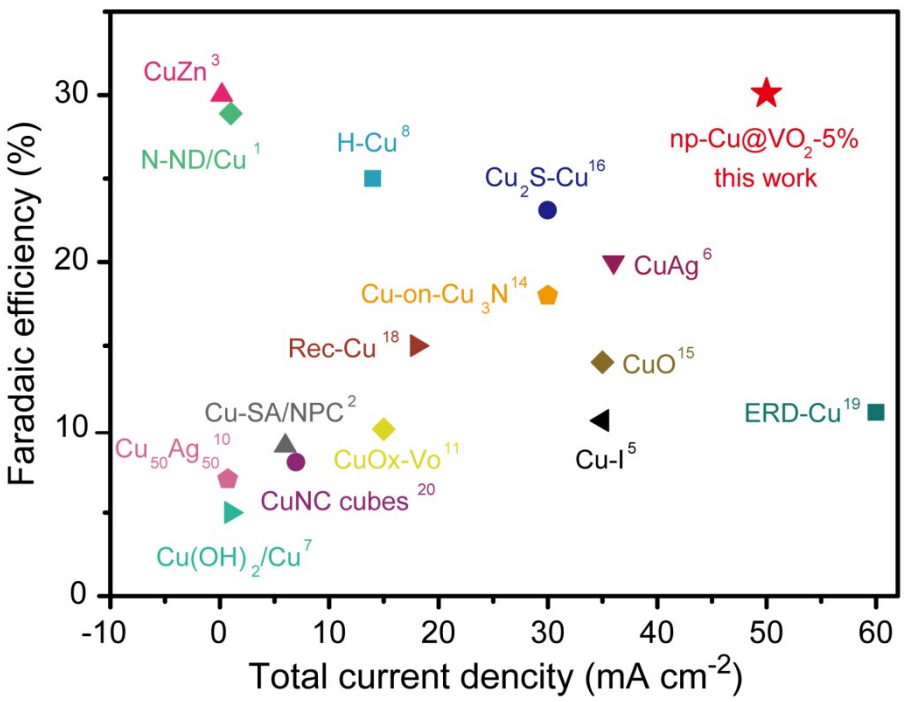


**Figure S16.** Ethanol Faradaic efficiency as a function of total current density on np-Cu@$VO_2$-5%, in comparison with other reports.

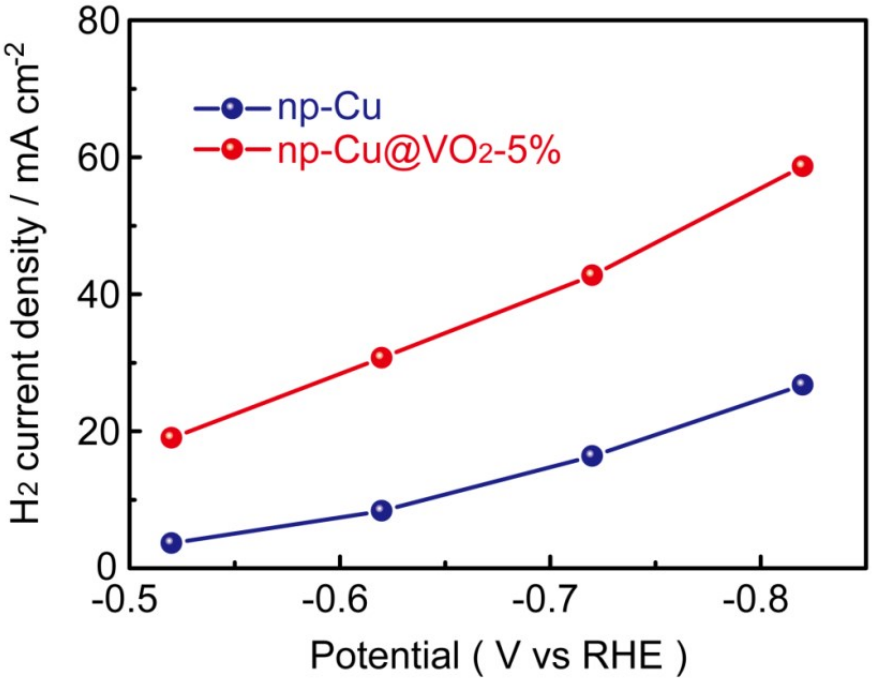


**Figure S17.** The comparison of $H_2$ current density between np-Cu and np-Cu@$VO_2$-5%.

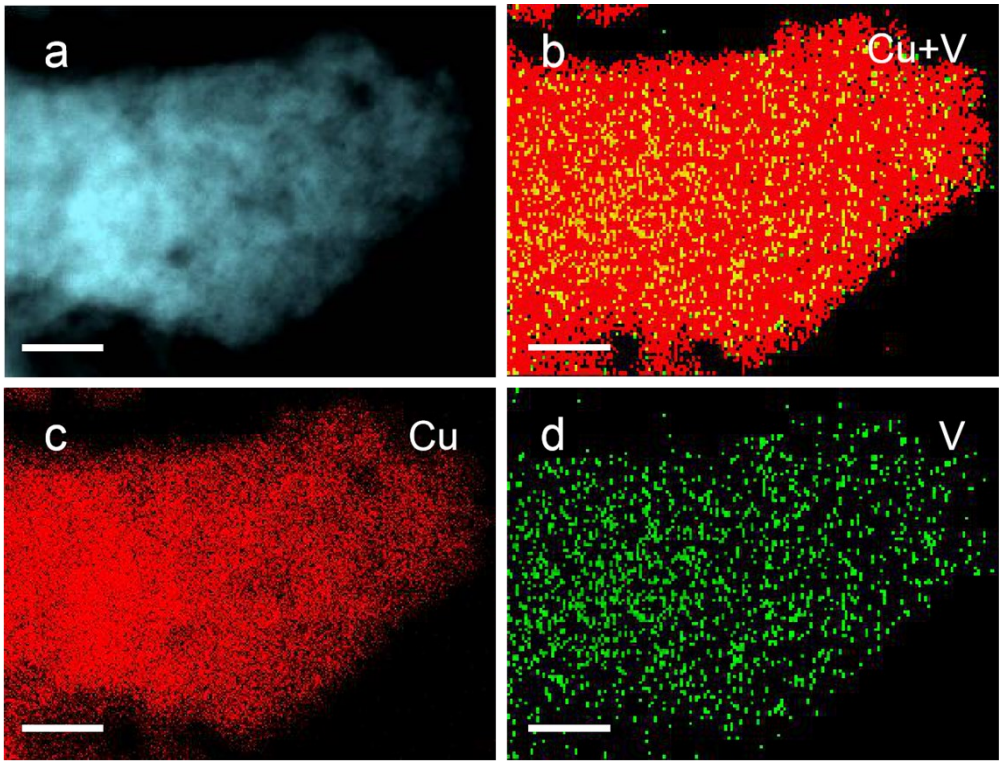


**Figure S18.** The STEM-EDS mappings of np-Cu@$VO_2$-5% after twelve hour of

carbon dioxide electroreduction test. (a) HADDF-STEM image. (b-d) Element mappings of (b) Overlapping of Cu and V, (c) Cu, and (d) V. Scale bars: (a-d) 20 nm.

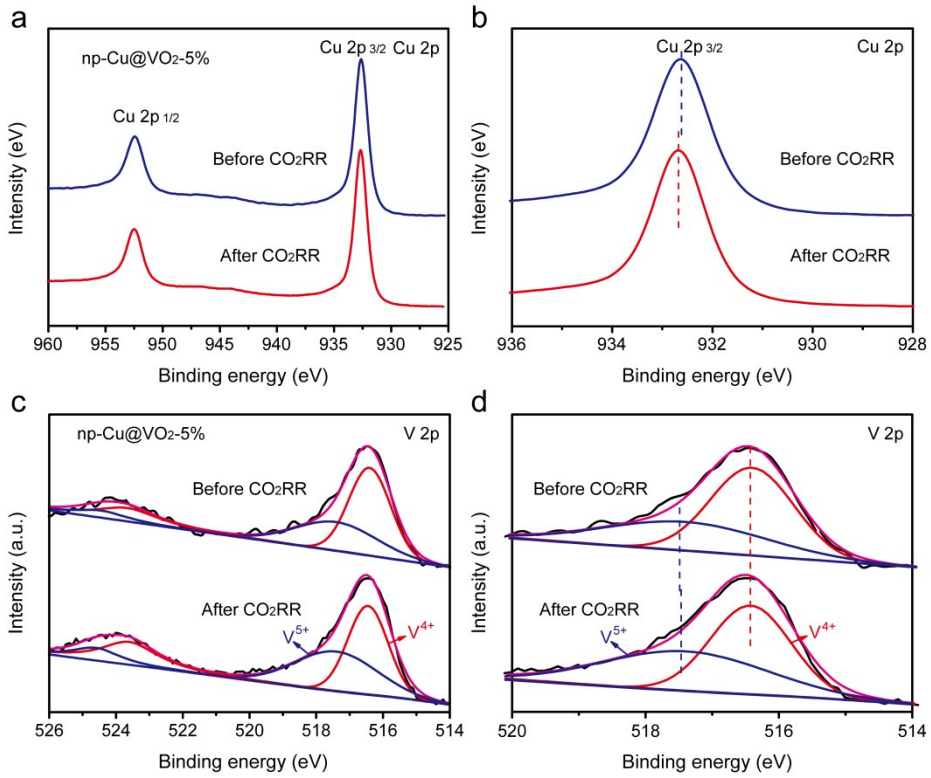


**Figure S19.** XPS spectrogram of np-Cu@$VO_2$-5% and np-Cu@$VO_2$-5% after stability test at a constant potential of -0.62 V *vs*. RHE (a) Cu 2p. (b) Cu 2p-amplification offset. (c) V 2p. (d) V 2p-amplification offset.

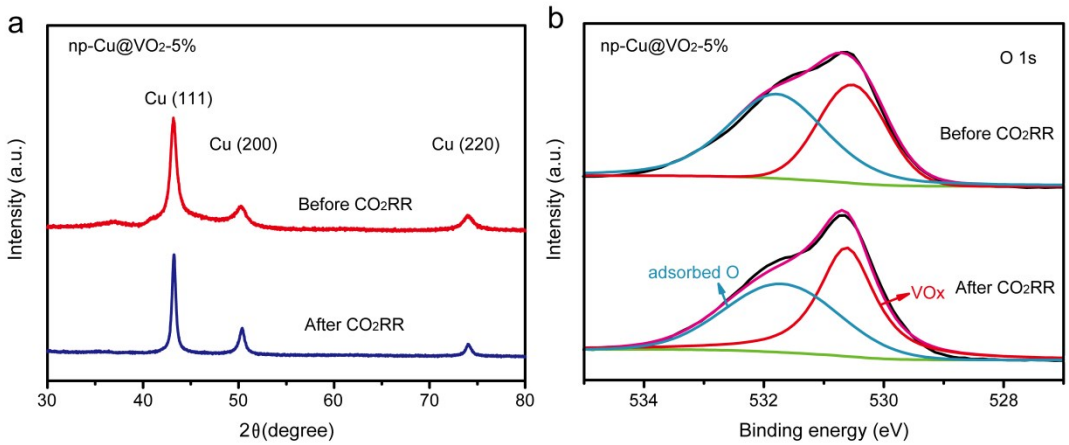

**Figure S20.** (a) XRD patterns and (b) O 1s XPS spectra for np-Cu@$VO_2$-5% before $CO_2$RR and after stability test of $CO_2$ reduction reaction.

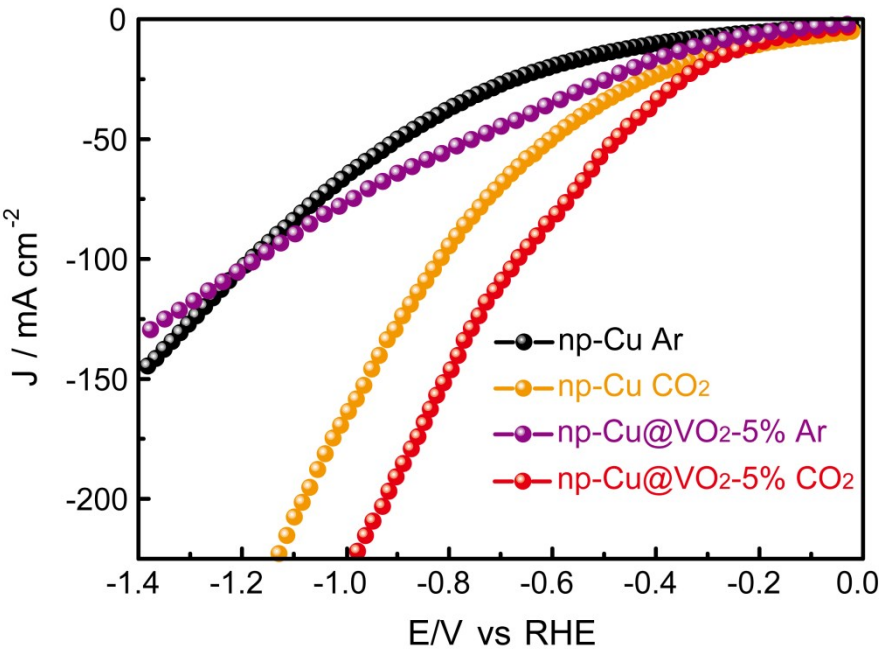


**Figure S21.** Polarization curves of np-Cu and np-Cu@$VO_2$-5% under Ar and $CO_2$ condition in Flow cell (Scan rate: 50 mV/s).

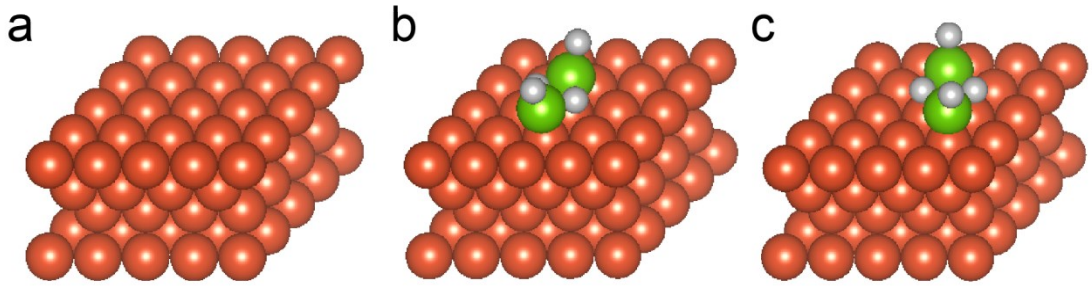


**Figure S22.** Density functional theory calculated model (a) Cu (111), (b) Cu@$VO_2$ (111), and (c) Cu@$VO_2$ (111) restructured after adsorption of *COOH in $CO_2$RR process. Red, white and green balls stand for copper, oxygen and vanadium atom, respectively.

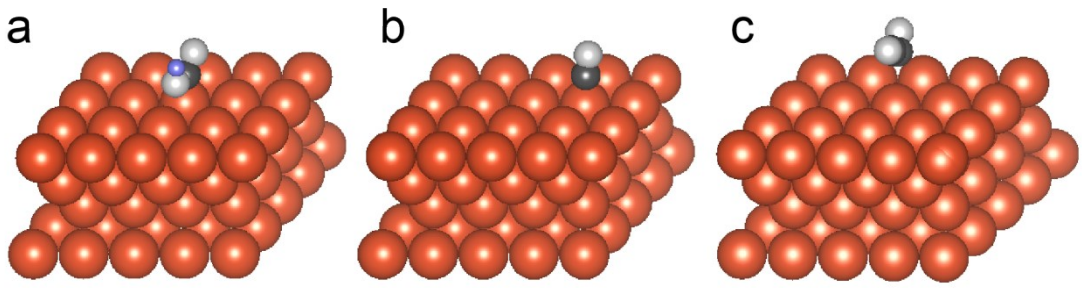


**Figure S23.** DFT calculated reaction state on Cu(111) mode. (a) *COOH adsorbed state, (b) *CO adsorbed state, and (c) *OCCO adsorbed state. Red, white, gray and blue balls stand for copper, oxygen, carbon, and hydrogen atom, respectively.

**Table S1.** Element composition for various catalyst derived from XPS test results.

| Catalyst | np-Cu@$VO_2$-1% | np-Cu@$VO_2$-5% | np-Cu@$VO_2$-10% | np-Cu@$VO_2$-5% after $CO_2$RR |
|---|---|---|---|---|
| Cu (atomic %) | 74.83 | 67.43 | 68.58 | 62.64 |
| V (atomic %) | 1.5 | 3.49 | 6.04 | 3.16 |
| O (atomic %) | 7.63 | 10.28 | 11.95 | 13.15 |
| C (atomic %) | 16.04 | 18.79 | 13.43 | 21.05 |

**Table S2.** Comparison of the $CO_2$ reduction performance of recently reported Cu-based electrocatalysts in H-type cell.

| **Catalyst** | **FE (EtOH, %)** | **E (V *vs.* RHE)** | **J(mA $cm^{-2}$)** | **Electrolyte** | **Ref.** |
|---|---|---|---|---|---|
| np-Cu@$VO_2$-5% | 30.1 | -0.62 | 50 | 0.1M KHCO3 | This work |
| N-ND/Cu | 28.9 | -0.5 | 1 | 0.1M KHCO3 | 1 |
| Cu-SA/NPC | 9 | -0.15 | 6 | 0.1M KHCO3 | 2 |
| CuZn | 30 | -1.15 | 0.2 | 0.1M KHCO3 | 3 |
| $Cu_{0.5}$NC | 43 | -1.2 | 38 | 0.1M CsHCO3 | 4 |

| | | | | | |
|---|---|---|---|---|---|
| Cu-I | 10.5 | -0.9 | 35 | 0.1M KHCO3 | 5 |
| CuAg | 20 | -1.05 | 36 | 0.2M KHCO3 | 6 |
| $Cu(OH)_2/Cu$ | 5 | -1 | 1 | 0.1M KHCO3 | 7 |
| H-Cu | 25 | -1.2 | 14 | 0.1M KHCO3 | 8 |
| $Cu\text{-}Cu_2O$ | 55 | -0.6 | 20 | 0.1M KHCO3 | 9 |
| $Cu_{50}Ag_{50}$ | 7 | -0.98 | 0.75 | 0.1M KHCO3 | 10 |
| CuOx-Vo | 10 | -1.2 | 15 | 0.1 M KHCO3 | 11 |
| 100cycle-Cu | 18 | -1.01 | 105 | 0.25 M KHCO3 | 12 |
| Cu-BDD | 42.4 | -0.4 | 0.1 | 0.5 M KCl | 13 |
| $Cu\text{-on-}Cu_3N$ | 18 | -0.94 | 30 | 0.1M KHCO3 | 14 |
| CuO | 14 | -0.95 | 35 | 0.1M KHCO3 | 15 |
| $Cu_2S$–Cu-V | 23.1 | -0.95 | 30 | 0.1M KHCO3 | 16 |
| Cu(B) | 27 | -1.1 | 70 | 0.1M KCl | 17 |
| Rec-Cu | 15 | -2 | 18 | 0.05M KHCO3 | 18 |
| ERD Cu | 11 | -1.1 | 60 | 0.1M KHCO3 | 19 |

| | | | | | |
|---|---|---|---|---|---|
| Cu NC cubes | 8 | -1.1 | 7 | 0.1M KHCO3 | 20 |

**Table S3.** Comparison of the $CO_2$ Reduction performance of recently reported Cu-based electrocatalysts in flow cell.

| Catalyst | FE(EtOH, %) | E(V *vs* RHE) | $J_{EtOH}$(mA/cm$^2$) | Electrolyte | Ref. |
|---|---|---|---|---|---|
| np-Cu@$VO_2$-5% | 38.2 | -0.8 | 39 | 1M KOH | This work |
| Cu(100) | 12 | -0.75 | 55 | 1M KOH | 21 |
| CuZn | 40 | -0.68 | 48 | 1M KOH | 3 |
| Cu-Ce$(OH)_x$ | 43 | -0.7 | 127 | 1M KOH | 22 |
| $Ag_{0.14}/Cu_{0.86}$ | 41 | -0.67 | 102 | 1M KOH | 23 |
| Cu | 4.5 | - | 11.2 | 1M $K_2CO_3$ | 24 |
| CuAg wire | 25 | -0.7 | 20 | 1M KOH | 25 |
| $Cu_2S$–Cu-V | 24.7 | < -2 | 98 | 1M KOH | 16 |
| Porous Cu | 20 | -0.67 | 128 | 1M KOH | 26 |
| Cu DAT-wire | 28 | -0.7 | 19.6 | 1M KOH | 27 |

| | | | | | |
|---|---|---|---|---|---|
| CuPd ordered | 15 | -0.65 | 39 | 1M KOH | 28 |

**Table S4.** Calculated adsorption energy of different intermediate in reaction path.

| Energy (eV) | $H_2O$ dissociation | $H_2O$ adsorption | H adsorption | *CO adsorption |
|---|---|---|---|---|
| Cu (111) | 0.4 | -0.42 | -0.28 | -0.62 |
| $V_2O_4$-Cu (111) | -0.93 | -1.46 | -0.5 | -0.67 |

**Table S5.** Calculated adsorption free energy of different intermediate species for $CO_2$RR.

| $CO_2$RR gibs energy (eV) | $CO_2$ | G (*COOH) | G (*CO) | G (*OCCO) |
|---|---|---|---|---|
| Cu (111) | 0 | 0.5 | -0.14 | 1.25 |
| $VO_2$-Cu (111) | 0 | 0.29 | 0.36 | 1.3 |

**References**


1. H. Wang, Y. Tzeng, Y. Ji, Y. Li, X. Zheng, A. Yang, Y. Liu, Y.Gong, L. Cai, Y. Li, X. Zhang, W. Chen, B. Liu, H. Lu, N. A. Melosh, Z. Shen, K. Chan, T. Tan, S. Chu, Y. Cui, *Nat. Nanotech.*, 2020, **15**, 131-137.

2. K. Zhao, X. Nie, H. Wang, S. Chen, X. Quan, H. Yu, W. Choi, G. Zhang, B. Kim, J. G. Chen, *Nat. Commun.*, 2020, **11**, 2455.

3. D. Ren, J. Gao, L. Pan, Z. Wang, J. Luo, S. M. Zakeeruddin, A. Hagfeldt, M. Gratzel, *Angew. Chem. Int. Ed.*, 2019, **58**, 15036-15040.

4. D. Karapinar, N. T. Huan, N. R. Sahraie, J. Li, D. Wakerley, N. Touati, S. Zanna, D. Taverna, L. H. G. Tizei, A. Zitolo, F. Jaouen, V. Mougel, M. Fontecave, *Angew. Chem. Int. Ed.*, 2019, **131**, 15242-15247.

5. D. Gao, I. Sinev, F. Scholten, R. M. Arán-Ais, N. J. Divins, K. Kvashnina, J. Timoshenko, B. R. Cuenya, *Angew. Chem. Int. Ed.*, 2019, **131**, 17203-17209.

6. J. Gao, H. Zhang, X. Guo, J. Luo, S. M. Zakeeruddin, D. Ren, M. Gratzel, *J. Am. Chem. Soc.*, 2019, **141**, 18704-18714.

7. G. Iijima, T. Inomata, H. Yamaguchi, M. Ito, H. Masuda, *ACS Catal.*, 2019, **9**, 6305-6319.

8. N. Suen, Z. Kong, C. Hsu, H. Chen, C. Tung, Y. Lu, C. Dong, C. Shen, J. Chung, H. Chen, *ACS Catal.*, 2019, **9**, 5217-5222.

9. Q.Zhu, X. Sun, D. Yang, J. Ma, X. Kang, L. Zheng, J. Zhang, Z. Wu, B. Han, *Nat. Commun.*, 2019, **10**, 3851.

10. D. Higgins, A. T. Landers, Y. Ji, S. Nitopi, C. G. Morales-Guio, L. Wang, K. Chan, C. Hahn, T. F. Jaramillo, *ACS Energy Lett.*, 2018, **3**, 2947-2955.

11. Z. Gu, N. Yang, P. Han, M. Kuang, B. Mei, Z. Jiang, J. Zhong, L. Li, G. Zheng, *Small Methods.*, 2018, 1800449.

12. K. Jiang, R. B. Sandberg, A. J. Akey, X. Liu, D. C. Bell, J. K. Norskov, K. Chan, H. Wang, *Nat. Catal.*, 2018, **1**, 111-119.

13. P. K. Jiwanti, K. Natsui, K. Nakata, Y.Einaga, *Electro. Acta.*, 2018, **266**, 414-419.

14. Z. Liang, T. Zhuang, A. Seifitokaldani, J. Li, C. Huang, C. Tan, Y. Li, P. D. Luna, C. T. Dinh, Y. Hu, Q. Xiao, P. Hsieh, Y. Wang, F. Li, R. Quintero-Bermudez, Y. Zhou, P. Chen, Y. Pang, S. Lo, L. Chen, H. Tan, Z. Xu, S. Zhao, D. Sinton, E. H. Sargent, *Nat. Commun.*, 2018, **9**, 3828.

15. D. Ren, J. Fong, B. S. Yeo, *Nat. Commun.*, 2018, **9**, 925.

16. T. Zhuang, Z. Liang, A. Seifitokaldani, Y. Li, P. D. Luna, T. Burdyny, F. Che, F. Meng, Y. Min, R. Quintero-Bermudez, C. T. Dinh, Y. Pang, M. Zhong, B. Zhang,

J. Li, P. Chen, X. Zheng, H. Liang, W. Ge, B. Ye, D. Sinton, S. Yu, E. H. Sargent, *Nat. Catal.*, 2018, **1**, 421-428.

17. Y. Zhou, F. Che, M. Liu, C. Zou, Z. Liang, P. D. Luna, H. Yuan, J. Li, Z. Wang, H. Xie, H. Li, P. Chen, E. Bladt, R. Quintero-Bermudez, T. Sham, S. Bals, J. Hofkens, D. Sinton, G. Chen, E. H.Sargent, *Nat. Chem.*, 2018, **10**, 974-980

18. M. G. Kibria, C. Dinh, A. Seifitokaldani, P. D. Luna, T. Burdyny, R. Quintero-Bermudez, M. B. Ross, O. S. Bushuyev, F. P. G. Arquer, P. Yang, D. Sinton, E. H. Sargent, *Adv. Mater.*, 2018, 1804867.

19. P. D. Luna, R. Quintero-Bermudez, C. Dinh, M. B.Ross, O. S. Bushuyev, P. Todorović, T. Regier, S. O. Kelley, P. Yang, E. H. Sargent, *Nat. Catal.*, 2018, **1**, 103-110.

20. A. Loiudice, P. Lobaccaro, E. A. Kamali, T. Thao, B. H. Huang, J. W. Ager, R. Buonsanti, *Angew. Chem. Int. Ed.*, 2016, **55**, 5789-5792.

21. Y. Wang, Z. Wang, C. Dinh, J. Li, A. Ozden, M. G. Kibria, A. Seifitokaldani, C. Tan, C. M. Gabardo, M. Luo, H. Zhou, F. Li, Y. Lum, C. McCallum, Y. Xu, M. Liu, A. Proppe, A. Johnston, P. Todorovic, T. Zhuang, D. Sinton, S. O. Kelley, E. H. Sargent, *Nat. Catal.*, 2020, **3**, 98-106.

22. M. Luo, Z. Wang, Y. C. Li, J. Li, F. Li, Y. Lum, D. Nam, B. Chen, J. Wicks, A. Xu, T. Zhuang, W. R. Leow, X. Wang, C. Dinh, Y. Wang, Y. Wang, D. Sinton, E. H. Sargent, *Nat. Commun.*, 2019, **10**, 5814.

23. Y. C. Li, Z. Wang, T. Yuan, D. Nam, M. Luo, J. Wicks, B. Chen, J. Li, F. Li, F. P. G. Arquer, Y. Wang, C. Dinh, O. Voznyy, D. Sinton, E. H. Sargent, *J. Am. Chem. Soc.*, 2019, **141**, 8584-8591.

24. Y. C. Li, G. Lee, T. Yuan, Y. Wang, D. Nam, Z. Wang, F. P. G. Arquer, Y. Lum, G. Dinh,, O. Voznyy, E. H. Sargent, *ACS Energy Lett.*, 2019, **4**, 1427-1431.

25. T. T. H. Hoang, S. Verma, S. Ma, T. T. Fister, J. Timoshenko, A. I. Frenkel, P. J. A. Kenis, A. A. Gewirth, *J. Am. Chem. Soc.*, 2018, **140**, 5791-5797.

26. J. Lv, M. Jouny, W. Luc, W. Zhu, J. Zhu, F. Jiao, *Adv. Mater.*, 2018, 1803111.

27. T. T. H. Hoang, S. Ma, J. I. Gold, P. J. A. Kenis, A. A. Gewirth, *ACS Catal.*, 2017, **7**, 3313-3321.

28. S. Ma, M. Sadakiyo, M. Heima, R. Luo, R. T. Haasch, J. I. Gold, M. Yamauchi, P. J. A. Kenis, *J. Am. Chem. Soc.*, 2017, **139**, 47-50.